Exciton fine structure and coherent spin precession in transition-metal-doped semiconductor quantum dots

A. K. Bhattacharjee
Laboratoire de Physique des Solides, UMR du CNRS, Université Paris-Sud, 91405 0rsay, France
(Received 21 February 2007; revised manuscript received 15 June 2007; published 3 August 2007)

The optical properties of quantum dots (QDs) containing a single magnetic impurity are studied within a multiband envelope function formalism. We present a unified treatment of different kinds of Mn-doped semiconductor QDs: spherical and ellipsoidal nanocrystals (NCs) and self-assembled quantum dots (SAQDs), focusing on their respective potentialities for optical detection and manipulation of the Mn spin state. The zero-field splitting of the exciton arising from the confinement-enhanced *sp-d* and electron-hole exchange interactions is deduced. The optical absorption spectrum shows a strong dependence on the Mn spin orientation with respect to the polarization of light, promising for optical detection. The theoretical results are in accord with the reported optical and magneto-optical properties of Mn-doped ZnSe NCs and CdTe/ZnTe SAQDs. Predictions for ellipsoidal wurtzite-structure CdSe NCs are also presented. Typically, NCs are smaller in size than SAQDs and show a correspondingly larger spin coupling and overall splitting. However, the splitting pattern is simpler in SAQDs, with fewer components, making for easier spin detection. The coherent precession of the Mn spin induced by a resonant circularly polarized laser pulse is also studied. A zero-field precession of substantial amplitude is obtained in nearly spherical NCs with strongly allowed hole-Mn spin flips. The amplitude is negligibly small in typical SAQDs, but the application of a transverse magnetic field (Voigt configuration) makes it measurable. Interestingly, in SAQDs containing a resident hole such as neutral GaAs:Mn or positively charged II-VI:Mn QDs, a significant zero-field spin precession of single frequency is predicted.

DOI: 10.1103/PhysRevB.76.075305 PACS number(s): 78.67.Hc, 71.70.Gm, 75.50.Pp, 78.47.+p

I. INTRODUCTION

Transition-metal-doped nanocrystals (NCs) or quantum dots (QDs) seem promising for possible applications in spintronics and quantum information processing. They belong to the family of diluted magnetic semiconductors (DMSs) with well-characterized carrier-ion spin interactions, which are strongly enhanced in QDs due to the confinement of carriers. Indeed, the formation of robust exciton magnetic polaron in different II-VI compound-based DMS QDs containing a substantial number of Mn ions has been reported in glass-embedded NCs[1] and self-assembled quantum dots (SAQDs).[2,3] The confinement effects seem even more spectacular in QDs containing a single Mn impurity.[4,5] Magnetic circular dichroism (MCD) measurements in Mn-doped colloidal ZnSe nanocrystals[6] indicated an order-of-magnitude enhancement of the giant Zeeman effect as compared with the bulk DMS of same Mn concentration. More recently, single-dot photoluminescence (PL) spectroscopy in Mn-doped CdTe/ZnTe SAQDs revealed a zero-field splitting of the exciton line into six bright components,[7] providing a rather direct evidence of the exciton-Mn spin coupling.

We previously developed a theoretical model based on the multiband envelope function formalism in the spherical approximation, which accounts for the optical and magneto-optical properties of DMS NCs.[8] In the dilute limit of a single Mn impurity in a QD, it provides an exact solution of the quantum-mechanical eigenvalue problem of an exciton (electron-hole pair) in interaction with the localized Mn spin.[9] Fully analytical in the case of spherical symmetry with Mn at the center of a nanocrystal, it was found to yield an excellent quantitative agreement with the experimental data of Ref. 6. The theory is here extended to cylindrical and lower symmetries which concern ellipsoidal/wurtzite NCs as well as self-assembled QDs. The departure from spherical symmetry in NCs is described perturbatively in terms of a uniaxial crystal-field-like term.[10,11] This model adequately accounts for the effects of exchange-induced mixing between the two doublets arising from the initially fourfold degenerate hole ground state. On the other hand, SAQDs are typically disklike and correspond to a relatively low in-plane confinement inside a narrow and strained quantum well. We, therefore, start from a cylindrically symmetric multiband model based on parabolic confinement.[12] The effects of the base-plane asymmetry are also considered.

Govorov and Kalameitsev[13] studied the optical properties of Mn-doped SAQDs within an elliptical disk model based on a simple heavy-hole valence band and proposed a mechanism for the manipulation of the Mn spin through resonant photoluminescence (PL). Fernández-Rossier[14] investigated the PL spectra in a multiband hard-wall rectangular box model.[15] Here, we present a generalized symmetry-based approach to different types of Mn-doped QDs including the SAQDs, which allows some analytical results. In addition to the spin Hamiltonian and the exciton fine structure spectrum, we calculate the coherent spin precession induced by a short circularly polarized laser pulse. A comparative discussion of the NCs and the SAQDs is presented, focusing on their respective potentialities for the optical detection and manipulation of the localized spin state.

The paper is organized as follows. In Sec. II, we derive the effective spin Hamiltonian for an exciton in interaction with a localized spin in different types of QDs. We next discuss its diagonalization and the optical absorption spectra

in each case in Sec. III including numerical results for Mn-doped CdSe NCs and asymmetric SAQDs. Section IV presents a study of the optically induced spin precession with or without an applied magnetic field. Finally, we sum up the main results and concluding remarks in Sec. V.

II. SPIN HAMILTONIAN

The *sp-d* exchange interaction between a band electron (spin $s=\frac{1}{2}$) and the Mn *d* electrons (total ionic spin $S=\frac{5}{2}$) located at $\mathbf{R}$ can be written as

$$\mathcal{H} = -J(\mathbf{r}-\mathbf{R})\mathbf{s}\cdot\mathbf{S}. \tag{1}$$

We follow the perturbation approach and study its effects on the confined electron (e) and hole (h) ground-state manifolds, by neglecting mixing with higher states. Indeed, even in a QD with a substantial number of Mn spins, the *sp-d* interaction induced contraction of the ground-state carrier wave functions is really small.[16] In small-size NCs, an exciton (electron-hole pair) can be approximately represented by the product wave functions: $\Psi^{e\text{-}h}_{m\mu}(\mathbf{r}_e,\mathbf{r}_h)=\psi^e_m(\mathbf{r}_e)\psi^h_\mu(\mathbf{r}_h)$. However, the excitonic correlation strongly affects the wave function in typical SAQDs, leading to a strong enhancement of the short-range *e-h* exchange interaction.[17] However, its effects on the *sp-d* exchange terms are expected to be small.

A. Nanocrystals

In a spherical nanocrystal of zinc blende semiconductors (T_d symmetry), the electron wave functions are $s=1/2$-like (Γ_6), and the hole wave functions (Γ_8) can be written as $j=3/2$ angular momentum eigenstates within the spherical approximation for the valence bands.[18]

$$\psi^e_m(\mathbf{r}) = \phi(\mathbf{r})u^c_m(\mathbf{r}), \tag{2}$$

with $\phi(\mathbf{r})=\sqrt{\frac{2}{a}}\frac{\sin(\pi r/a)}{r}Y_{00}$, where a is the NC radius, $u^c_m(\mathbf{r})$ the conduction band Bloch function at Γ, and $m=s_z=\pm\frac{1}{2}$.

$$\psi^h_\mu(\mathbf{r}) = \sum_\nu F_{\nu\mu}(\mathbf{r})u^h_\nu(\mathbf{r}), \tag{3}$$

where μ, ν run through $\frac{3}{2}$, $\frac{1}{2}$, $-\frac{1}{2}$, and $-\frac{3}{2}$. $u^h_\nu(\mathbf{r})$ are the time-reversed valence-band Bloch functions at Γ, with $j_z=\nu$. Here, we consider the dipole-active fourfold ground state $1S_{3/2}$ that corresponds to $F_{\nu\mu}(\mathbf{r})=\delta_{\nu\mu}R_0(r)Y_{00}+\langle\frac{3}{2},\nu;2,(\mu-\nu)\big|\frac{3}{2},\mu\rangle R_2(r)Y_{2,\mu-\nu}(\theta,\varphi)$. The radial functions $R_0(r)$ and $R_2(r)$ are linear combinations of spherical Bessel functions: $R_0(r)=C[j_0(kr/a)-\kappa j_0(kr\sqrt{\delta}/a)]$ and $R_2(r)=-C[j_2(kr/a)+\kappa j_2(kr\sqrt{\delta}/a)]$. Here, C is the normalization constant, $\kappa\equiv j_0(k)/j_0(k\sqrt{\delta})$, with k given by the lowest solution of $j_2(k)j_0(k\sqrt{\delta})+j_0(k)j_2(k\sqrt{\delta})=0$. Note that the hole energy is $E_0=\hbar^2(\gamma_1-2\gamma)(k/a)^2/(2m_0)$, where $\gamma\equiv(2\gamma_2+3\gamma_3)/5$. Also, $\delta\equiv(\gamma_1-2\gamma)/(\gamma_1+2\gamma)$. $\{\gamma_i\}$ are the Luttinger parameters and m_0 is the free-electron mass.

Now,

$$\langle\psi^e_m|\mathcal{H}|\psi^e_n\rangle = -\alpha|\phi(R)|^2\langle m|\mathbf{s}\cdot\mathbf{S}|n\rangle, \tag{4}$$

where $|m\rangle$ is an eigenstate of s_z and $\alpha=\langle u_s|J(\mathbf{r})|u_s\rangle$, with $|u_s\rangle$ for the *s*-like orbital wave function. Similarly,

$$\langle\psi^h_\mu|\mathcal{H}|\psi^h_\nu\rangle = -\frac{\beta}{3}\sum_{\lambda,\xi}F^*_{\lambda,\mu}(\mathbf{R})\langle\lambda|\mathbf{j}\cdot\mathbf{S}|\xi\rangle F_{\xi,\nu}(\mathbf{R}), \tag{5}$$

where $|\lambda\rangle$ is an eigenstate of j_z $\left(j=\frac{3}{2}\right)$ and $\beta=\langle u_x|J(\mathbf{r})|u_x\rangle$. The Mn spin is described in terms of the $S_z=M_S$ eigenstates. The matrix elements of the *sp-d* exchange Hamiltonian in the *e-h* subspace can thus be written in terms of a spin Hamiltonian by choosing the quantization axis z along $\mathbf{R}$: $H_{sp\text{-}d}=H_0+H_A$, with the isotropic part

$$H_0 = -I_e(\mathbf{s}\cdot\mathbf{S}) - I_h(\mathbf{j}\cdot\mathbf{S}), \tag{6}$$

where $I_e=\alpha|\phi(R)|^2$ and $I_h=(\beta/3)|f(R)|^2\left[1-\frac{5}{4}t(R)\right]^2$, respectively, correspond to *e*-Mn and *h*-Mn (isotropic part) exchange interactions. Here, α and β are the bulk exchange parameters, $f(r)\equiv R_0(r)/\sqrt{4\pi}$ and $t(r)\equiv R_2(r)/R_0(r)$. The anisotropic part

$$H_A = -I_h\rho[\{j_z^2(\mathbf{j}\cdot\mathbf{S})+(\mathbf{j}\cdot\mathbf{S})j_z^2\}+\rho\{j_z^2(\mathbf{j}\cdot\mathbf{S})j_z^2\}], \tag{7}$$

where $\rho=t(R)/\left[1-\frac{5}{4}t(R)\right]$. Note that ρ vanishes at the NC center and its magnitude increases slowly with increasing R (see Ref. 19 for the quantitative variation of the exchange parameters with R in ZnSe:Mn NCs). An off-center position of the Mn impurity reduces the symmetry of the spin Hamiltonian from spherical to cylindrical.

The short-range *e-h* exchange interaction is given by

$$H_{eh} = -I_{eh}(\mathbf{s}\cdot\mathbf{j}), \tag{8}$$

with $I_{eh}=c\hbar\omega_{ST}\chi(\delta)(a_B/a)^3$. Here, $c=2$ (3/2) for wurtzite (zinc blende) crystals, a_B the bulk exciton Bohr radius, and $\hbar\omega_{ST}$ the singlet-triplet splitting.[11]

However, even with Mn at the NC center, the approximate symmetry is no longer spherical but cylindrical if the NC is ellipsoidal and/or the crystal structure is wurtzite. In both cases,[11] the $j=3/2$-like hole ground-state quartet splits into two doublets, $|j_z|=3/2$ and $|j_z|=1/2$, which can be described by a uniaxial crystal-field model,

$$H_{CF} = -(D/2)(j_z^2-9/4), \tag{9}$$

where D depends on the size and the ellipticity of the NC. Clearly, the axial symmetry will hold for the spin Hamiltonian as long as Mn is on the symmetry axis.

B. Self-assembled quantum dots

Another case of approximate axial symmetry arises in self-assembled QDs. *A priori* belonging to D_{2d} symmetry, they are usually modeled by a confinement potential of cylindrical symmetry. We shall use the model of Ref. 12, which assumes a finite square-well potential along the growth axis (z) and a harmonic oscillator for lateral confinement. The electron envelope functions can then be written as a product of a subband wave function $f(z)$ and a two-dimensional (2D) harmonic oscillator wave function,

$$\psi^e_{n,l,m}(\mathbf{r}) = \sum_s c_s f_s(z)F_{n,l}(\rho,\phi)u^c_m(\mathbf{r}), \tag{10}$$

where c_s is a normalization constant and

$$f_s(z) = \sqrt{\frac{2}{W}} \sin\left(\frac{s\pi[z + W/2]}{W}\right). \tag{11}$$

Here, W is larger than the width w of the square well (QW). Note that in the case of infinite depth, no summation is necessary: $f_s(z)$ with $W=w$ become the eigenstates. The 2D harmonic oscillator eigenfunctions are given by

$$F_{n,l}(\rho,\phi) = B_{nl}(i\rho)^{|l|} e^{-\rho^2/2a^2} e^{il\phi} L_n^{|l|}(\rho^2/a^2), \tag{12}$$

where $L_n^{|l|}$ is the generalized Laguerre polynomial and B_{nl} the normalization constant.[12] Note that the lateral confinement radius a is now related to the force constant and the in-plane carrier effective mass.

The hole wave functions are obtained in the axial approximation for the valence band. The resulting cylindrical symmetry assures that $j_z=\mu$, the sum of the envelope angular momentum l and the band-edge value ν, is a good quantum number. Thus,

$$\psi_\mu^h(\mathbf{r}) = \sum_{\nu,n,s} C_{n,s,\nu}^{\mu} F_{n,\mu-\nu}(\rho,\phi) f_s(z) u_\nu^h(\mathbf{r}). \tag{13}$$

The confined hole states $|\mu|=1/2,3/2,5/2,\ldots$ are doubly degenerate due to time-reversal symmetry and contain contributions from both heavy-hole (hh) and light-hole (lh) valence-band states. Parity is also a good quantum number as the inversion asymmetry terms in the $\mathbf{k}\cdot\mathbf{p}$ Hamiltonian are neglected. Typically, under low lateral confinement, the hole ground state is $S_{3/2}^+$ of even parity.[12] Note that the oscillator functions in Eq. (13) refer to the in-plane hh effective mass: $m_h=m_0/(\gamma_1+\gamma_2)$. If lh-hh mixing is neglected, they become the lowest-energy eigenstates. In the general case, the 4×4 Luttinger Hamiltonian needs to be diagonalized in this basis to obtain the eigenstates.

As for the *sp-d* terms of the spin Hamiltonian, we note that the electron part remains isotropic: $H_e=-I_e\mathbf{s}\cdot\mathbf{S}$ with $I_e=[\alpha/(\pi a_e^2)]\exp(-\rho_0^2/a_e^2)|\Sigma c_s f_s(z_0)|^2$, where $\mathbf{R}=(z_0,\rho_0,\phi_0)$. For deducing the hole part, we first *assume* that the Mn site is on the growth axis: $\mathbf{R}=(z_0,0,0)$. By noting that $F_{n,l}(0,0)=(1/a\sqrt{\pi})\delta_{l0}$, we obtain

$$\langle\psi_\mu^h|\mathcal{H}|\psi_\nu^h\rangle = -I_h^{\mu\nu}(\mathbf{j}_{\mu\nu}\cdot\mathbf{S}), \tag{14}$$

where

$$I_h^{\mu\nu} = (\beta/3)[1/(\pi a_h^2)] \sum_{m,s,n,t} C_{m,s,\mu}^{\mu *} C_{n,t,\nu}^{\nu} f_s^*(z_0) f_t(z_0).$$

Thus, the hole-Mn coupling retains the cylindrical symmetry and has nonvanishing matrix elements only for hole states with $|j_z|=1/2$ and $3/2$. The matrix elements depend on the projection of the QD state $|\psi_\mu^h\rangle$ on the band state u_μ^h, for both initial and final states. Generally speaking, this weight factor depends on $|\mu|$ and varies with the QD size, so that we have three coupling constants for dealing with the typical case where the ground state is $j_z=\pm3/2$ and the first excited one $j_z=\pm1/2$. Only in the small-size limit (strong lateral confinement) are the weight factors roughly equal and close to unity,[20] leading to the isotropic Heisenberg form $-I_h\mathbf{j}\cdot\mathbf{S}$ as in NCs. On the other hand, in large-size QDs with low in-plane confinement, such as the ones studied experimentally,[7] the *sp-d* exchange splitting is much smaller than the separation between the two hole levels. Limiting to the $j_z=\pm3/2$ ground-state doublet, the *h*-Mn Hamiltonian for on-axis Mn reduces to the Ising form

$$H_h = -I_h j_z S_z, \tag{15}$$

where $I_h=I_h^{\mu\mu}$ with $\mu=3/2$.

Note, however, that even in the ground-state subspace $(S_{3/2}^+)$, spin-flip terms appear in H_h when the magnetic impurity is not on the z axis. Those are due to the lh-hh mixing in the QD hole wave functions. Considering the mixing in the lowest order of perturbation, we obtain

$$\psi_{3/2}^h(\mathbf{r}) = f_1(z)[F_{0,0}(\rho,\phi)u_{3/2}^h(\mathbf{r}) + CF_{0,2}(\rho,\phi)u_{-1/2}^h(\mathbf{r})]. \tag{16}$$

Similarly, its time-reversed partner $\psi_{-3/2}^h(\mathbf{r})$ contains a small admixture of the lh band state $u_{+1/2}^h(\mathbf{r})$. Note that we have assumed unmixed wave functions of the lowest order with $n=0$ and $s=1$ only. Within the model of Ref. 12, it can be shown that $C\simeq-(\gamma\sqrt{6}/\gamma_2)(w/2\pi a)^2$. Thus, up to the first order in C, we have $\langle\pm3/2|\mathcal{H}|\pm3/2\rangle=\mp(3/2)I_h^0S_z$ and $\langle3/2|\mathcal{H}|-3/2\rangle=-\epsilon I_h^0S_-$. Here, $I_h^0=(2/\pi w a_h^2)\times(\beta/3)\cos^2(\pi z_0/w)\exp(-\rho_0^2/a_h^2)$ and $\epsilon\equiv C\sqrt{3/2}(\rho_0/a_h)^2\exp(-2i\phi_0)$. By choosing the x axis to pass through the Mn site, $\phi_0=0$, and the effective hole-Mn spin Hamiltonian can be written in a symmetric form in terms of the $\tilde{j}=1/2$ pseudospin operators,

$$H_h' = -3I_h^0\left[\tilde{j}_z S_z + \frac{2}{3}\epsilon(\tilde{j}_x S_x + \tilde{j}_y S_y)\right]. \tag{17}$$

In the present model of a cylindrically symmetric QD, the spin-flip terms arising from lh-hh band mixing appear only when the Mn impurity is off axis so that the spin Hamiltonian is no longer axially symmetric. A similar mixing term was previously obtained for on-center Mn in a laterally asymmetric $(L_x\neq L_y)$ rectangular QD.[15,14] If the band mixing is altogether neglected, the *h*-Mn spin Hamiltonian is of the Ising form, independent of the QD shape or Mn position.[13]

The short-range *e-h* exchange interaction retains the Ising form $H_{eh}=-I_{eh}s_z j_z$, but a quantitative calculation of I_{eh} in terms of $\hbar\omega_{ST}$ calls for that of the exciton wave function.[17] Moreover, quantum wells and related SAQDs often contain base-plane asymmetry and the uniaxial model cannot account for the so-called *xy* splitting in the exciton fine structure, which arises from the asymmetric terms, dominated by the long-range exchange interaction.[21] We, therefore, resort to the standard form of the generalized *e-h* Hamiltonian,[22]

$$H_{eh} = -\sum_i [a_i s_i j_i + b_i s_i j_i^3], \tag{18}$$

where the sum runs over (x,y,z).

III. EIGENVALUES AND OPTICAL ABSORPTION SPECTRUM

Here, we discuss the diagonalization of the spin Hamiltonian, which yields the energies and relative intensities of

the exciton components. Analytical results will be presented first.

A. Nanocrystals

With the magnetic impurity at the center of a spherical NC, the effective spin Hamiltonian $H=H_0+H_{eh}$ commutes with the total angular momentum $\mathbf{J}=\mathbf{s}+\mathbf{j}+\mathbf{S}$, so that its eigenvalues and eigenstates can be deduced analytically by using the theory of addition three angular momenta.[9] With $s=1/2$, $j=3/2$ and $S=5/2$, we obtain a total of eight energy levels: $J=1/2(1)$, $3/2(2)$, $5/2(2)$, $7/2(2)$, $9/2(1)$, where the number in the parentheses shows the number of levels. Note that the two levels $J=1/2$ and $J=9/2$ are electric-dipole forbidden for optical transitions, because they have no projection of the $j_{\mathrm{ex}}=1$ exciton states. The two energy levels for a given J are

$$\Lambda_{\pm}^{J}=\frac{1}{4}(I_e-I_h+I_{eh})-\frac{I_h}{2}\left[\left(J+\frac{1}{2}\right)^2-\left(S+\frac{1}{2}\right)^2-\left(j+\frac{1}{2}\right)^2\right]\pm\frac{1}{2}\left[\left(J+\frac{1}{2}\right)^2(I_e-I_h)(I_{eh}-I_h)+\left(S+\frac{1}{2}\right)^2(I_e-I_h)(I_e-I_{eh})+\left(j+\frac{1}{2}\right)^2(I_e-I_{eh})(I_h-I_{eh})\right]^{1/2}. \quad (19)$$

The eigenstates can be written as

$$|J,\pm,M\rangle=C_1^{\pm}\left|S+\tfrac{1}{2},j,J,M\right\rangle+C_2^{\pm}\left|S-\tfrac{1}{2},j,J,M\right\rangle, \quad (20)$$

with $C_1^{+}=\sin\phi$, $C_2^{+}=\cos\phi$, $C_1^{-}=\cos\phi$, $C_2^{-}=-\sin\phi$, where $\tan\phi\equiv H_{12}/(\Lambda_{+}-H_{11})$ (see Ref. 9 for the matrix elements of H).

In order to deduce the optical absorption spectrum, let us note that the initial state of the system is that of the paramagnetic ion spin, with the QD valence-band states fully occupied. The spin state can be either a prepared pure (coherent) state or a mixed state describing thermodynamic equilibrium. In either case it can be treated in terms of the eigenstates of S_z. Thus, without any loss of generality, we consider $|i\rangle=|M_S\rangle$ for the initial state. By neglecting the magnetic dipole interaction with the electromagnetic field, the spin state remains unchanged in optical transitions. On the other hand, the possible final states $|f\rangle$ are the eigenstates of H deduced above. It is easy to see that, in the electric-dipole approximation, the relative oscillator strengths of the six allowed transitions are

$$P^{J\pm}(m)=|\langle J,\pm,M|m,M_S\rangle|^2, \quad (21)$$

where $|m,M_S\rangle\equiv|1,m\rangle|M_S\rangle$ with the $j_{\mathrm{ex}}=1$ exciton states,[9] the m values characterizing the polarization of light. Note that in the final state, $M=m+M_S$. As an example, with $M_S=-5/2$, in polarization σ_-, $M=-7/2$ and we have only two transitions corresponding to $\Lambda_{+}^{7/2}$ and $\Lambda_{-}^{7/2}$, with relative intensities given by $I_{\pm}=|(-\frac{3}{2\sqrt{6}})C_1^{\pm}+(\frac{\sqrt{15}}{2\sqrt{6}})C_2^{\pm}|^2$. The same results hold for $M_S=5/2$ and σ_+, i.e., Mn spin parallel to the exciton spin (see Ref. 9 for the full spectrum in ZnSe NCs in different configurations and magnetic fields, which accounted for the experimental MCD data).

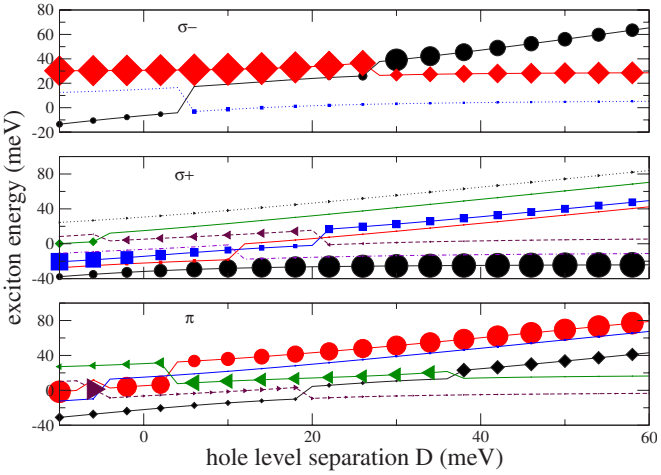

FIG. 1. (Color online) Zero-field exciton components in an ellipsoidal wurtzite-structure CdSe NC of "radius" of 2 nm with Mn impurity at the center with its spin oriented antiparallel to the z axis ($S_z=-5/2$). The energy is plotted against the hole level separation D. The three panels, from top to bottom, respectively, correspond to σ_-, σ_+, and π polarizations. The size of the symbols indicates the relative oscillator strength.

For an off-center impurity ($\mathbf{R}\neq 0$) in a spherical NC, we have axial symmetry around the $\mathbf{R}$ direction and M is a good quantum number but not J, so that the energy levels enumerated above split. In general, H needs to be diagonalized numerically (see below). However, for Mn site quite far from the center, $|\rho|$ remains small, and it is adequate to approximate H_A by the term in the first order of ρ and treat it as a perturbation with respect to H_0. The resulting correction can be deduced analytically,

$$\Delta_{\pm}^{JM}=-I_h\rho[\gamma(a_1,a_2)+\gamma(b_1,b_2)M^2], \quad (22)$$

where $\gamma(x,y)=(C_1^{\pm})^2(U+A)x-C_1^{\pm}C_2^{\pm}\sqrt{AB}(x+y)+(C_2^{\pm})^2(U+B)y$. Here, $a_1(a_2)=1(2)$, $31/16(11/8)$, $3/2(1/2)$ and $b_1(b_2)=1/5(-3/5)$, $-33/140$ $(-3/70)$, $-1/21(1/7)$ for $J=3/2$, $5/2$, $7/2$, respectively. Note that U, A, and B are explicitly given in Ref. 9.

In the case of a wurtzite and/or ellipsoidal NC, the spin Hamiltonian remains axially symmetric as long as Mn lies on the c axis. Once again, M is a good quantum number. The Hamiltonian matrix thus takes a block-diagonal form with blocks of dimensions 1, 3, 5, 7, and 8, respectively, for $M=\pm 9/2$, $\pm 7/2$, $\pm 5/2$, $\pm 3/2$, and $\pm 1/2$. The effects of mixing between the ground- and excited-state hole doublets induced by the sp-d exchange couplings were studied numerically. As $|D|$ increases from zero, each $\Lambda_{\pm}^{J}$ energy level splits into the components $|M|$. With further increase of $|D|$, we obtain the crossing and anticrossing of levels and finally a progressive separation of the subspaces belonging to the two doublets.

In Fig. 1, we present some results for the zero-field optical absorption spectra in CdSe:Mn NCs of radius $a=2$ nm with Mn close to the center (see Ref. 23 about the synthesis of such NCs). The relevant NC parameters are $I_e=2.88$ meV,

TABLE I. Zero-field exciton components in a symmetric SAQD containing a single Mn atom for different values of S_z in the ground state. The zero of energy is the fundamental gap of the undoped QD with $I_{eh}=0$. The brighter (darker) component in each case, designated by the superscript b (d), corresponds to the + (−) sign on the right-hand side.

S_z	σ_+	σ_-
5/2	$E^{b,d}_{\sigma+}=\frac{1}{4}I_e-3I_h\pm\frac{1}{2}\sqrt{(2I_e-\frac{3}{2}I_h+\frac{3}{2}I_{eh})^2+5I_e^2}$	$E^{b}_{\sigma-}=-\frac{5}{4}I_e+\frac{15}{4}I_h+\frac{3}{4}I_{eh}$
3/2	$E^{b,d}_{\sigma+}=\frac{1}{4}I_e-\frac{3}{2}I_h\pm\frac{1}{2}\sqrt{(I_e-\frac{3}{2}I_h+\frac{3}{2}I_{eh})^2+8I_e^2}$	$E^{b,d}_{\sigma-}=\frac{1}{4}I_e+3I_h\pm\frac{1}{2}\sqrt{(2I_e+\frac{3}{2}I_h-\frac{3}{2}I_{eh})^2+5I_e^2}$
1/2	$E^{b,d}_{\sigma+}=\frac{1}{4}I_e\pm\frac{1}{2}\sqrt{(\frac{3}{2}I_h-\frac{3}{2}I_{eh})^2+9I_e^2}$	$E^{b,d}_{\sigma-}=\frac{1}{4}I_e+\frac{3}{2}I_h\pm\frac{1}{2}\sqrt{(I_e+\frac{3}{2}I_h-\frac{3}{2}I_{eh})^2+8I_e^2}$

$I_h=-5.85$ meV, and $I_{eh}=4.39$ meV, based on the bulk parameters $N_0\alpha=0.26$ eV, $N_0\beta=-1.11$ eV, and $\hbar\omega_{ST}=0.13$ meV. According to Ref. 11, D in ellipsoidal CdSe NCs roughly varies from −5 to +50 meV. We show the spectrum for the initial state $S_z=-5/2$ over a slightly wider range. The three panels from top to bottom correspond to the exciton spin parallel (σ_-), antiparallel (σ_+), and perpendicular (π) to the Mn spin. Here, the relative oscillator strengths are shown by the size of the symbols. After the initial level crossings and transfer of oscillator strengths, for $D>40$ meV, we have essentially two bright lines in each circular polarization: the stronger (weaker) one in the ground (excited)-state subspace. At the same time, the π polarization shows two components of almost equal intensity in the lh-like upper subspace.

B. Self-assembled quantum dots

Here, typically the *sp-d* exchange coupling is much smaller than the hole level separation, and we focus on the ground-state doublet $|j_z|=3/2$. Let us first neglect all departure from uniaxial symmetry: off-axis impurity and/or in-plane asymmetry. Then, both j_z and M are good quantum numbers, even with a magnetic field (B) along z. Using the basis $\{|j_z,s_z,S_z\rangle\}$ it is then easy to see that for a given M value, we have two uncoupled 2×2 matrices to diagonalize,

$$H^{\pm}_{11}=\pm\frac{1}{2}I_e(M\mp1)\mp\frac{3}{2}I_h(M\mp1)+\frac{3}{4}I_{eh}+B\mu_B\left[g_{\mathrm{Mn}}(M\mp1)\mp\frac{1}{2}g_e\mp\frac{3}{2}g_h\right], \quad (23a)$$

$$H^{\pm}_{12}=-\frac{1}{2}I_e\sqrt{S(S+1)-(M\mp1)(M\mp2)}, \quad (23b)$$

$$H^{\pm}_{22}=\mp\frac{1}{2}I_e(M\mp2)\mp\frac{3}{2}I_h(M\mp2)-\frac{3}{4}I_{eh}+B\mu_B\left[g_{\mathrm{Mn}}(M\mp2)\pm\frac{1}{2}g_e\mp\frac{3}{2}g_h\right], \quad (23c)$$

with $|1\rangle_\pm=|\pm3/2,\mp1/2,M\mp1\rangle$ and $|2\rangle_\pm=|\pm3/2,\pm1/2,M\mp2\rangle$. Here, the subscripts ± correspond to $\sigma_\pm$ excitons, with the bright exciton states $|j^z_{\mathrm{ex}}=j_z+s_z=\pm1\rangle$ weakly coupled to the dark ones $|j^z_{\mathrm{ex}}=\pm2\rangle$ through *e*-Mn exchange. The solution is thus analytical, yielding 12 doubly degenerate energy levels at $B=0$, of which one ($M=\pm9/2$) is electric-dipole forbidden. Explicitly, the eigenstates for the $\{M,\sigma\pm\}$ manifold are $|b\rangle=\cos\theta|1\rangle_\pm+\sin\theta|2\rangle_\pm$ and $|d\rangle=-\sin\theta|1\rangle_\pm+\cos\theta|2\rangle_\pm$, with $\tan\theta\equiv H^{\pm}_{12}/(E_b-H^{\pm}_{22})$. Here, b (d) corresponds to the brighter (darker) component, with the relative intensity $\cos^2\theta$ ($\sin^2\theta$). It is interesting to note that the eigenstates correspond to circularly polarized optical transitions.

We explicitly calculate the spectrum for a given value of S_z. The zero-field components are shown in Table I. Note that the σ_+ (σ_-) component for $S_z=-M_S$ is degenerate with the σ_- (σ_+) component for $S_z=M_S$. Clearly, contrary to the assumption in Ref. 24, the energy separation between the brighter components for a given value of S_z is not generally proportional to $|S_z|$. The relative intensities of optical transitions for different S_z values and circular polarizations follow from the eigenstates, as in the case of NCs. The optical detection of the Mn spin state in a symmetric SAQD seems particularly simple: for instance, if $S_z=5/2$, the energy separation between the σ_+ and σ_- lines will be given by $\Delta\equiv E^b_{\sigma+}-E^b_{\sigma-}$, the overall zero-field splitting of the brighter components.

This symmetric hh model accounted for the PL and magneto-PL data in Ref. 7, giving a good fit with $I_e=0.067$ meV, $I_h=-0.111$ meV, and $I_{eh}=0.67$ meV. In the absence of any precise characterization of the QDs, a quantitative modelization cannot be carried out. Yet, we have made a consistency check by using the lowest-order envelope functions ($n=0,l=0,s=1$), assuming the suggested[7] QD height: $w=3$ nm. The above I_e value will then correspond to $I^0_e=2\alpha/(\pi w a_e^2)$ for on-center Mn. By using the bulk CdTe:Mn parameters,[16] we thus obtain $a_e=6.885$ nm. Now, $(a_h/a_e)^2=\sqrt{m_e(\gamma_1+\gamma_2)}$ so that $a_h=6.035$ nm, yielding $I^0_h=-0.116$ meV, which is indeed close to the empirical I_h value. The observed difference[7] between the exchange parameter ratio I_h/I_e and its bulk counterpart $\beta/(3\alpha)$ is thus explained by the different carrier confinement lengths.

C. Asymmetric self-assembled quantum dots

In QDs with base-plane anisotropy, both *h*-Mn and *e-h* exchange interactions contribute terms of lower symmetry, so that M is no longer a good quantum number and a numerical diagonalization is necessary. Both terms lead to a finite linear polarization of the zero-field components. Typically, the hole-Mn spin-flip terms are much smaller than the asymmetric *e-h* exchange terms in Eq. (18). In Fig. 2, we present numerical results for such a system. In particular, we

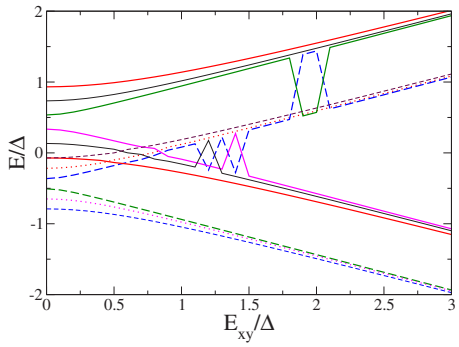

FIG. 2. (Color online) Exciton components in an asymmetric QD. The energy is plotted against the *xy* splitting, both scaled to the overall *sp-d* splitting △. The parameters used (see text) are suitable for CdTe/ZnTe QDs. The solid (broken) lines correspond to the brighter (darker) components.

plot the energy of the zero-field heavy-hole exciton components as a function of the asymmetry splitting $E_{xy}=(3/4)\times(b_x-b_y)$, both scaled to the overall *sp-d* splitting Δ. We have assumed $I_e=0.1$ meV, $I_h=-0.2$ meV, and $a_z=1.0$ meV, of the same order of magnitude as in Ref. 7. The six solid (broken) lines correspond to the brighter (darker) components. Note how the exciton fine structure evolves from six almost equidistant circularly polarized components toward two linearly polarized triplets, after passing through some interesting level crossings and/or anticrossings. The increasing value of the ratio E_{xy}/Δ may correspond to a decrease of the *sp-d* exchange with the distance of Mn from the center and/or an increase of the in-plane anisotropy.[13,24]

IV. SPIN PRECESSION

Optical manipulation of the Mn spin state in SAQDs through resonant photoluminescence has been proposed in Ref. 13. Here we consider the coherent spin precession induced by the absorption of a short circularly polarized laser pulse, presumably observable in time-resolved pump-probe Faraday or Kerr rotation spectroscopy, a well-established technique succesfully applied in DMS quantum wells for probing spin coherence.[25] With the eigenstates of the coupled exciton-Mn system on hand, it is straightforward to calculate the spin precession. We assume a resonant excitation by an ultrashort laser pulse with its peak frequency at the center of the exciton spectrum and its spectral width larger than the overall splitting. Suppose that the Mn spin is initially oriented along $\mathbf{n}(\theta,\varphi)$, i.e., $|S_n=S\rangle=\Sigma D^{(S)}_{\mu,S}(\varphi,\theta,0)|\mu\rangle$, where $D^{(S)}$ represents the rotation matrix. The σ_+ photon pulse creates an exciton with $j^z_{\rm ex}=1$, where z is the direction of light propagation, coinciding with the symmetry axis. The state of the system at $t=0$ is then $|\Psi(0)\rangle=|j^z_{\rm ex}=1\rangle|S_n=S\rangle$. This is a coherent superposition of the eigenstates $\{|p\rangle\}$ covered by the pulse width: $|\Psi(0)\rangle=\Sigma_p c_p|p\rangle$ and $|\Psi(t)\rangle=\exp\left(-\frac{i}{\hbar}Ht\right)|\Psi(0)\rangle$. Thus, the time-dependent expectation value of the z component of the Mn spin,

$$\langle S_z\rangle(t)=\sum_{p,q} c^*_p c_q\langle p|S_z|q\rangle\exp(i\omega_{pq}t), \tag{24}$$

where $\omega_{pq}=(E_p-E_q)/\hbar$. The exciton spin will also undergo simultaneous precession so that the resultant total M remains constant in time (in cylindrical symmetry). However, the precession of the resultant magnetic moment, dominated by the Mn spin, should remain observable through the Faraday or Kerr rotation. Note that, in the absence of a transverse magnetic field (see below), the driving mechanism for this precession is the *sp-d* exchange interaction, more precisely, its spin-flip terms. In the mean-field description, the light-induced exchange field is oriented along z and cannot lead to any time evolution of $\langle S_z\rangle$. As the exciton spin relaxation time in a DMS QD is known to be longer than the recombination time,[3] we expect the zero-field spin precession to last until the recombination. Obviously, for a quantitative description of the coherent spin dynamics in a QD ensemble, it is necessary to solve the corresponding master equation, incorporating the spin relaxation and recombination times.[26] Here, we limit the discussion to a single QD and calculate $\langle S_z\rangle(t)$, in order to discern the basic characteristics of spin precession.

A. Zero-field precession

Before presenting numerical results, let us first consider a simple case: $|S_z=5/2\rangle$ for the initial state. After σ_+ resonant excitation, $|\Psi(0)\rangle$ is a linear combination of the dipole-allowed exciton components belonging to $M=7/2$.

In the case of spherical NCs, only the two $J=7/2$ energy levels are concerned. We obtain

$$\langle S_z\rangle(t)=5/2-A\sin^2\omega t, \tag{25}$$

where $\hbar\omega=(\Lambda^{7/2}_+-\Lambda^{7/2}_-)/2$ and $A=(\sin 2\phi+\sqrt{15}\cos 2\phi)/36$, with ϕ as defined above. In ZnSe:Mn NCs of diameter of 5.3 nm (see Ref. 9 for the parameters), $A=0.296$ and $\hbar\omega=5.77$ meV, which calls for femtosecond spectroscopy. Note that this energy is inversely proportional to the NC volume and in ellipsoidal NCs can be also tuned through D.

On the other hand, in the case of cylindrical SAQDs, we have the same equation for $\langle S_z\rangle(t)$ with $A=\sin^2 2\theta$, with θ above. For instance, in the case of CdTe:Mn QDs of Ref. 7, we obtain $A=0.0131$ and $\hbar\omega=0.65$ meV. The amplitude of precession is thus dramatically smaller in SAQDs, as it is driven by the much weaker *e*-Mn coupling alone.

However, a particularly interesting case is that of a SAQD containing a resident hole, e.g., GaAs:Mn or InAs:Mn, where Mn is known to be an acceptor. The situation is qualitatively similar in a positively charged II-VI:Mn QD. In such a system, the ground state is doubly degenerate $\{j_z=\pm 3/2,\ S_z=\mp 5/2\}$. If the initial state is $|j_z=-3/2,\ S_z=5/2\rangle$, the only allowed excitation is σ_+ leading to $|\Psi(0)\rangle=|j^1_z+j^2_z=0\rangle|s_z=-1/2\rangle|S_z=5/2\rangle$, corresponding to the two-hole ground state with effectively compensated hole spin.[12,27] It is then a linear combination of the eigenstates of coupled *e*-Mn system with $M=2$: $|\Psi(0)\rangle=c_1|S+\frac{1}{2},M\rangle+c_2|S-\frac{1}{2},M\rangle$. A straightforward calculation gives

$$\langle S_z\rangle(t)=5/2-(5/9)\sin^2(3I_e/2\hbar)t, \tag{26}$$

with a substantial relative amplitude. Note that in the case of SAQD with a resident electron, with the initial state $|s_z=1/2,\ S_z=5/2\rangle$, the allowed excitation is σ_+ and the ex-

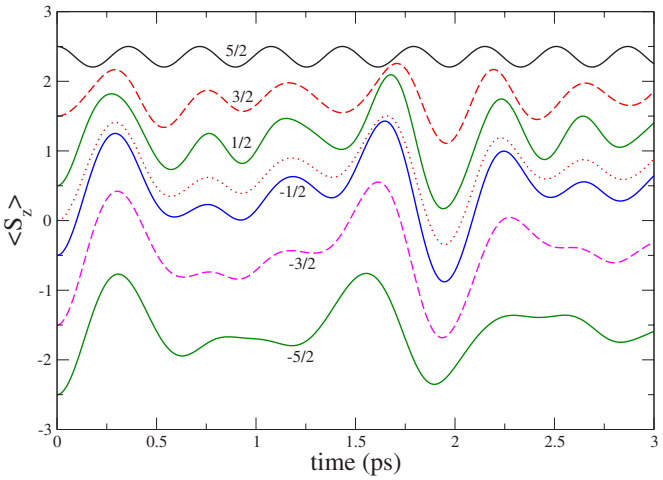

FIG. 3. (Color online) Zero-field spin precession in a ZnSe NC of diameter of 5.3 nm under resonant excitation by a short σ_+ pulse for different initial states. The curves are labeled by the initial values of S_z. The unlabeled dotted curve starting at $\langle S_z\rangle=0$ corresponds to the initial states $S_x=\pm 5/2$.

cited state an eigenstate of the hole-Mn system, which precludes any spin precession.

In the three simple cases considered above, the optical excitation connects only two energy levels and the spin precession has a single frequency, as in typical QW systems. However, generally speaking, for other initial orientations of spin, we have a sum of several terms of different frequencies and amplitudes, giving a more complicated behavior, as illustrated in Fig. 3, which shows $\langle S_z\rangle(t)$ under σ_+ excitation in ZnSe NCs of diameter of 5.3 nm for different initial states of the Mn spin. Note that the incoherent time-average value, $\overline{\langle S_z\rangle}\equiv\Sigma_p|c_p|^2\langle p|S_z|p\rangle$, gives a measure of the overall precession amplitude. For instance, we obtain $\overline{\langle S_z\rangle}=-1.561$ and $+0.708$, respectively, for $S_z(0)=-5/2$ and $S_x(0)=\pm 5/2$.

In wurtzite and/or ellipsoidal NCs such as CdSe:Mn discussed above, we find that $|\overline{\langle S_z\rangle}-\langle S_z\rangle(0)|$ decreases with increasing $|D|$ toward zero. This results from a progressive freezing of hole-Mn spin flips through the increasing separation between the light- and heavy-hole-like subspaces, as seen in Fig. 1. Obviously, SAQDs qualitatively correspond to the asymptotic limit.

B. Precession in the presence of a magnetic field

Let us consider a magnetic field B along x, perpendicular to the direction of light propagation (Voigt configuration). At low temperatures, the initial state of the Mn spin can be readily prepared as $S_x=-5/2$. Now, the spin precession under σ_+ excitation results from the combined effects of the *sp-d* exchange and the Zeeman Hamiltonian. Once again, we just need to calculate the full eigenspectrum in order to deduce $\langle S_z\rangle(t)$ from Eq. (24). We present numerical results in Fig. 4 for the SAQDs, where the application of a magnetic field is seen to drastically enhance the precession amplitude. Note that, in addition to the exchange parameters for CdTe:Mn QDs quoted above, we used $g_{\mathrm{Mn}}=2$, $g_h^{\perp}\simeq 0$, and $g_e=-1.5$.[7]

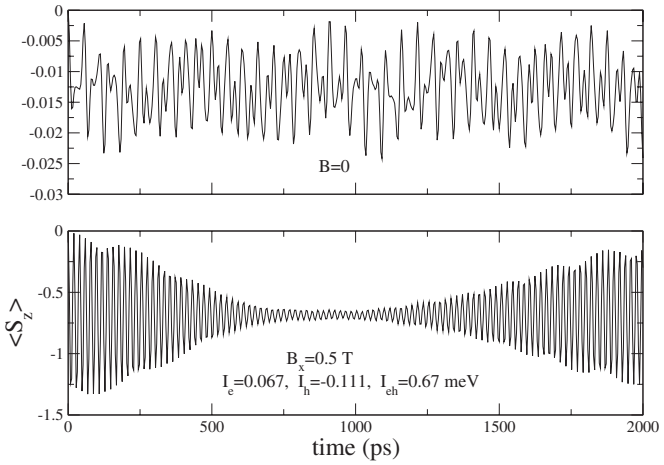

FIG. 4. Spin precession in a CdTe/ZnTe QD under resonant excitation by a short σ_+ pulse for the initial spin state $S_x=-5/2$. The upper (lower) panel corresponds to $B=0$ ($B_x=0.5$ T).

The zero-field precession of the Mn spin, exclusively arising from its coupling with the exciton spin, stops at the recombination time $t=\tau$, assumed shorter than the exciton spin relaxation time. However, in the presence of a magnetic field, the precession continues. At $t>\tau$, the Hamiltonian of the system is given by $H_Z=g_{\mathrm{Mn}}\mu_B BS_x$ and $|\Psi(t)\rangle=\exp\left(-\frac{i}{\hbar}H_Z[t-\tau]\right)|\Psi(\tau)\rangle$. Recalling the operator for rotation about the x axis, we have

$$\langle S_z\rangle(t)=\langle S_z\rangle(\tau)\cos\Theta(t)+\langle S_y\rangle(\tau)\sin\Theta(t), \qquad (27)$$

where $\Theta(t)=(t-\tau)g_{\mathrm{Mn}}\mu_B B/\hbar$. The precession frequency is now that of the Mn EPR and the amplitude is related to the exciton-induced tilting of the spin at $t=\tau$. The results are illustrated in Fig. 5 for CdTe:Mn SAQDs. Note that the complex multifrequency precession pattern sometimes leads to a progressively decreasing amplitude over a substantial time

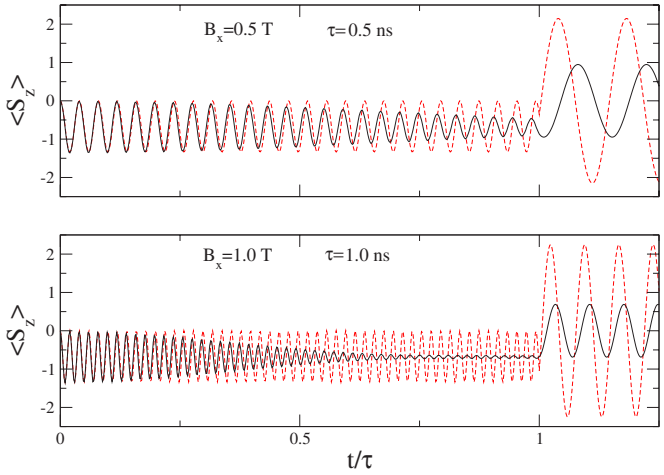

FIG. 5. (Color online) Optically induced spin precession in a CdTe/ZnTe QD as in Fig. 4, including the effects of exciton recombination. The upper (lower) panel corresponds to the field $B_x=0.5$ (1.0) T and the recombination time $\tau=0.5$ (1.0) ns. The broken lines show the mean-field results.

interval, which corresponds to a low-frequency envelope, rather than a loss of coherence.

For comparison, we also present the mean-field approximation (MFA) results, where the exciton-Mn exchange interaction is treated as an effective field $B_{\mathrm{ex}}=\left(\frac{1}{2}I_e-\frac{3}{2}I_h\right)/(g_{\mathrm{Mn}}\mu_B)$ in the z direction acting on the magnetic moment $\mathbf{M}=-g_{\mathrm{Mn}}\mu_B\mathbf{S}$ initially oriented along x by the applied field B. The resulting precession of $\mathbf{M}$ around the total field $\mathbf{B}_t=B_{\mathrm{ex}}\hat{\mathbf{z}}+B\hat{\mathbf{x}}$ leads to

$$\langle S_z\rangle_{MFA}(t)=-\frac{5}{2}\left(\frac{BB_{\mathrm{ex}}}{B_t^2}\right)2\sin^2\left(\frac{\omega t}{2}\right), \tag{28}$$

for $t\leqslant\tau$, with $\hbar\omega=g_{\mathrm{Mn}}\mu_B B_t$. The time evolution after recombination ($t>\tau$) is again given by Eq. (27). The MFA results are indicated by the broken lines in Fig. 5: they obviously correspond to a single frequency even before recombination, which roughly coincides with the highest frequency ($\Delta/\hbar$) of the exact solution.

V. CONCLUDING REMARKS

We have presented a unified description of the optical properties of Mn-doped QDs of different symmetries: spherical and/or ellipsoidal NCs and epitaxial SAQDs. A multiband envelope function formalism is used to derive the spin Hamiltonian of an exciton in interaction with the Mn^{2+} ion, including its position dependence. As expected, the spin Hamiltonian for an off-center (off-axis) impurity in a spherical (cylindrical) QD has a lower symmetry. In SAQDs of cylindrical symmetry with low in-plane confinement where the Ising Hamiltonian holds for the h-Mn coupling for on-axis Mn, we obtain a position-dependent lh-hh mixing term for off-axis Mn which allows h-Mn spin flips. Such a mixing term was previously associated with the base-plane anisotropy alone. The latter, however, leads to stronger effects through the e-h exchange interaction, which is typically much larger than the sp-d exchange.

We next diagonalized the spin Hamiltonian, obtaining the excitonic energy levels and wave functions, the latter yielding the relative oscillator strengths of the optical transitions. The results which are analytical in the symmetric cases are explicitly shown. Our results for spherical NCs and cylindrical SAQDs were found to provide a good agreement with the experimental data in ZnSe NCs and CdTe/ZnTe SAQDs, respectively. We have also presented numerical results for the zero-field exciton splitting in ellipsoidal wurtzite-structure CdSe NCs.

The optical absorption spectrum strongly depends on the orientation of the Mn spin with respect to the light polarization. The results suggest that optical spin detection should be easier to realize in highly ellipsoidal NCs or SAQDs, where the number of low-energy bright components is fewer than that in quasispherical NCs. In fact, in the former systems, we have essentially one bright component in each circular polarization for a given value of S_z. This idyllic situation, however, does not prevail in the low-symmetry cases, where the anisotropic e-h exchange terms and/or the h-Mn spin-flip ones give rise to multicomponent linearly polarized transitions.

Our study of the zero-field light-induced coherent precession of the Mn spin shows that the amplitudes are substantial only in quasispherical NCs with strongly allowed h-Mn spin flips. However, the multicomponent nature of the quantum beats might lead to complications in the interpretation of the relevant pump-probe experiments. A particularly interesting case arises in SAQDs with a resident hole such as positively charged II-VI:Mn QDs or neutral GaAs:Mn QDs, where a significant zero-field precession of single frequency is predicted. The corresponding quantum beats could possibly be probed also through time-resolved PL experiments.

In the presence of a transverse magnetic field (Voigt configuration), we predict a measurable spin precession in neutral II-VI SAQDs, which evolve to the simple Mn EPR behavior after exciton recombination. Hopefully, our results would be helpful to future experimental studies aimed at realizing the optical detection and manipulation of the localized spin states in semiconductor QDs.

[1] K. Yanata, K. Suzuki, and Y. Oka, J. Appl. Phys. **73**, 4595 (1993); K. Yanata and Y. Oka, Jpn. J. Appl. Phys., Suppl. **34**, 164 (1995).

[2] A. A. Maksimov, G. Bacher, A. McDonald, V. D. Kulakovskii, A. Forchel, C. R. Becker, G. Landwehr, and L. Molenkamp, Phys. Rev. B **62**, R7767 (2000).

[3] S. Mackowski, T. Gurung, T. A. Nguyen, H. E. Jackson, L. M. Smith, G. Karczewski, and J. Kossut, Appl. Phys. Lett. **84**, 3337 (2004).

[4] R. N. Bhargava, D. Gallagher, X. Hong, and A. Nurmikko, Phys. Rev. Lett. **72**, 416 (1994).

[5] D. M. Hoffman, B. K. Meyer, A. I. Ekimov, I. A. Merkulov, Al. L. Efros, M. Rosen, G. Couino, T. Gacoin, and J. P. Boilot, Solid State Commun. **114**, 547 (2000).

[6] D. J. Norris, N. Yao, F. T. Charnok, and T. A. Kennedy, Nano Lett. **1**, 3 (2001).

[7] L. Besombes, Y. Léger, L. Maingault, D. Ferrand, H. Mariette, and J. Cibert, Phys. Rev. Lett. **93**, 207403 (2004).

[8] A. K. Bhattacharjee, Phys. Rev. B **51**, 9912 (1995).

[9] A. K. Bhattacharjee and J. Pérez-Conde, Phys. Rev. B **68**, 045303 (2003).

[10] A. K. Bhattacharjee, in *Semiconductor Heteroepitaxy: Growth, Characterization and Device Applications*, edited by B. Gil and R.-L. Aulombard (World Scientific, Singapore, 1995), p. 126.

[11] Al. L. Efros, M. Rosen, M. Kuno, M. Nirmal, D. J. Norris, and M. Bawendi, Phys. Rev. B **54**, 4843 (1996).

[12] F. B. Pedersen and Y.-C. Chang, Phys. Rev. B **53**, 1507 (1996); **55**, 4580 (1997).

[13] A. O. Govorov and A. V. Kalameitsev, Phys. Rev. B **71**, 035338 (2005).

[14] J. Fernández-Rossier, Phys. Rev. B **73**, 045301 (2006).
[15] F. V. Kyrychenko and J. Kossut, Phys. Rev. B **70**, 205317 (2004).
[16] A. K. Bhattacharjee and C. Benoit à la Guillaume, Phys. Rev. B **55**, 10613 (1997).
[17] R. Romestain and G. Fishman, Phys. Rev. B **49**, 1774 (1994).
[18] P. C. Sercel and K. J. Vahala, Phys. Rev. B **42**, 3690 (1990); Al. L. Efros, *ibid.* **46**, 7448 (1992).
[19] A. K. Bhattacharjee and J. Pérez-Conde, Phys. Status Solidi B **241**, 672 (2004).
[20] K. Chang, S. S. Li, J. B. Xia, and F. M. Peeters, Phys. Rev. B **69**, 235203 (2004).
[21] E. L. Ivchenko, Phys. Status Solidi A **164**, 487 (1997).
[22] M. Bayer, A. Kuther, A. Forchel, A. Gorbunov, V. B. Timofeev, F. Schäfer, J. P. Reithmaier, T. L. Reinecke, and S. N. Walck, Phys. Rev. Lett. **82**, 1748 (1999).
[23] S. C. Erwin, L. Zu, M. I. Haftel, Al. L. Efros, T. A. Kennedy, and D. J. Norris, Nature (London) **436**, 91 (2005).
[24] Y. Léger, L. Besombes, L. Maingault, D. Ferrand, and H. Mariette, Phys. Rev. Lett. **95**, 047403 (2005).
[25] S. A. Crooker, D. D. Awschalom, J. J. Baumberg, F. Flack, and N. Samarth, Phys. Rev. B **56**, 7574 (1997); D. D. Awschalom and N. Samarth, in *Semiconductor Spintronics and Quantum Computation*, edited by D. D. Awschalom, D. Loss, and N. Samarth (Springer-Verlag, Berlin, 2002), p. 147.
[26] M. Linder and L. J. Sham, Physica E (Amsterdam) **2**, 412 (1998).
[27] J. I. Climente, M. Korkusinski, P. Hawrylak, and J. Planelles, Phys. Rev. B **71**, 125321 (2005).